

Model-independent tracking of criticality signals in nuclear multifragmentation data

J. D. Frankland,¹ A. Chbihi,¹ A. Mignon,¹ M. L. Begemann-Blaich,² R. Bittiger,² B. Borderie,³ R. Bougault,⁴ J.-L. Charvet,⁵ D. Cussol,⁴ R. Dayras,⁵ D. Durand,⁴ C. Escano-Rodriguez,¹ E. Galichet,^{3,6} D. Guinet,⁷ P. Lantesse,⁷ A. Le Févre,² R. Legrain,^{5,*} N. Le Neindre,³ O. Lopez,⁴ J. Łukasik,^{2,8} U. Lynen,² L. Manduci,⁴ J. Marie,⁴ W. F. J. Müller,² L. Nalpas,⁵ H. Orth,² M. Pârlog,⁹ M. Pichon,⁴ M. F. Rivet,³ E. Rosato,¹⁰ R. Roy,¹¹ A. Saija,² C. Schwarz,² C. Sfienti,² B. Tamain,⁴ W. Trautmann,² A. Trzcinski,¹² K. Turzó,² A. Van Lauwe,⁴ E. Vient,⁴ M. Vigilante,¹⁰ C. Volant,⁵ J. P. Wieleccko,¹ and B. Zwieglinski¹²

(INDRA and ALADIN Collaborations)

¹*GANIL, CEA et IN2P3-CNRS, Boîte Postale 55027, F-14076 Caen Cedex, France*

²*Gesellschaft für Schwerionenforschung mbH, D-64291 Darmstadt, Germany*

³*Institut de Physique Nucléaire, IN2P3-CNRS, F-91406 Orsay Cedex, France*

⁴*LPC, IN2P3-CNRS, ENSICAEN et Université, F-14050 Caen Cedex, France*

⁵*DAPNIA/SPhN, CEA/Saclay, F-91191 Gif sur Yvette Cedex, France*

⁶*Conservatoire National des Arts et Métiers, F-75141 Paris Cedex 03, France*

⁷*Institut de Physique Nucléaire, IN2P3-CNRS et Université, F-69622 Villeurbanne, France*

⁸*Institute of Nuclear Physics, PL-31342 Kraków, Poland*

⁹*National Institute for Physics and Nuclear Engineering, RO-76900 Bucharest-Măgurele, Romania*

¹⁰*Dipartimento di Scienze Fisiche e Sezione INFN, Università di Napoli "Federico II," I-80126 Napoli, Italy*

¹¹*Laboratoire de Physique Nucléaire, Université Laval, Québec, Canada*

¹²*Soltan Institute for Nuclear Studies, PL-00681 Warsaw, Poland*

(Received 21 April 2004; published 28 March 2005)

We look for signals of criticality in multifragment production in heavy-ion collisions using model-independent universal fluctuations theory. The phenomenon is studied as a function of system size, bombarding energy, and impact parameter over a wide range of INDRA data. For very central collisions ($b/b_{\max} < 0.1$) we find evidence that the largest fragment in each event, Z_{\max} , plays the role of an order parameter, defining two different regimes at low and high incident energy, respectively, according to the scaling properties of its fluctuations. Data for a wide range of system masses and incident energies collapse on to an approximately universal scaling function in each regime for the most central collisions. The forms of the scaling functions for the two regimes are established, and their dependence on the total mass and the bombarding energy is mapped out. Data suggest that these regimes are linked to the disappearance of heavy residues in central collisions.

DOI: 10.1103/PhysRevC.71.034607

PACS number(s): 25.70.Pq

I. INTRODUCTION

It has long been hoped that the study of nuclear multifragmentation reactions as observed in intermediate-energy heavy-ion collisions [1–5] can give valuable information on the nuclear matter phase diagram and equation of state [6–8]. The principal guidewire for this research has been the search for signs of something analogous to a liquid-gas phase transition in data on intermediate mass fragment (IMF) production, ever since the observation of power laws in fragment mass-yield distributions [9,10], reminiscent of the condensation of liquid drops in a critical vapor [11]. This effort was encouraged by the failure of statistical models of hot nuclear decay [12–14] to explain the observed fragment yields [2,15] unless they suppose the breakup of the system at low densities [16–18] where the phase transition may occur [6].

Signals of the phase transition in experimental data on multifragmentation may be revealed by anomalously large fluctuations of fragment observables [19–21]. The main obstacles to such endeavors insofar as experimental data are

concerned are the huge statistical fluctuations inherent to small systems such as atomic nuclei and the still-open question of the mechanism(s) of fragment production in heavy-ion collisions at intermediate energies [22–39]. Indeed in all experimental studies of the question, at the same time as one is searching for evidence of the phase transition of a piece of hot nuclear matter [35], one is (implicitly or not) obliged to elucidate the manner in which such an excited system may be formed in the course of certain reactions [34]. The solidity of any experimental evidence for a link between multifragmentation and the nuclear matter phase diagram will be undermined by any remaining ambiguity about the dominant mechanism of fragment production in the selected sample of experimental events, and it would be preferable to be able to address the question of “phases” in nuclear multifragmentation independently of reaction mechanism.

It is for this reason that the theory of the universal character of order parameter fluctuations in finite systems proposed by Botet and Płoszajczak [40–43] provides an attractive opportunity to address the question of phase transitions induced by heavy-ion collisions in the least ambiguous way possible. According to their work, it is possible to obtain pertinent information on the relationship between the formation of

*Deceased.

clusters in a system and the phase transition(s) of said system without needing to characterize the state of the system under study to the extent of, for example, supposing it to be in thermodynamical equilibrium at the time of cluster formation. One needs only to study the properties of the clusters: specifically, all pertinent information can be obtained from a sufficiently precise measurement of the event-by-event distributions of cluster multiplicity and the size of the largest cluster produced. The attractiveness of such an approach in the domain of nuclear fragmentation reactions is obvious, for the reasons just given. Although the mechanism of fragment production remains an open question, for several years now large solid-angle multidetector arrays such as INDRA have provided high-quality data on the multiplicity and the size (charge) of the fragments produced in such reactions.

A first application of the universal fluctuations theory to INDRA data for central collisions of Xe + Sn from 25A to 50A MeV was published in [44]. In this paper we will present the results of the same analysis applied to a wide range of systems measured with INDRA. As in [44] we observe a signature compatible with the existence of different regimes at different bombarding energies. This behavior disappears for less central collisions. By applying the analysis to data for colliding systems with total mass number between 73 and 394 we will show the mass dependence of the energy of transition between the two regimes and present a systematic study of the universal scaling functions observed in the low- and high-energy regimes.

II. UNIVERSAL FLUCTUATIONS OF THE ORDER PARAMETER IN FINITE SYSTEMS

Universal scaling laws of fluctuations (the Δ -scaling laws) have been derived for equilibrium systems and have been shown to apply also in certain out-of-equilibrium situations. In a system in which the second-order critical behavior can be identified, the relation among order parameter, criticality, and scaling law of fluctuations has been established and the relation between the scaling function and the critical exponents has been found. Details can be found in [43].

Experimental observables that may be related to a critical order parameter can be identified through their Δ -scaling behavior. The Δ scaling is observed when two or more probability distributions $P_N[m]$ of the observable m for a system of “size” N collapse onto a single scaling curve $\Phi(z_{(\Delta)})$ independent of system size when plotted in terms of the scaling variables:

$$\langle m \rangle^\Delta P_N[m] = \Phi(z_{(\Delta)}) = \Phi\left(\frac{m - \langle m \rangle}{\langle m \rangle^\Delta}\right), \quad (1)$$

where $\langle m \rangle$ is the mean value of the distribution $P_N[m]$ and $1/2 \leq \Delta \leq 1$. Here $\langle m \rangle$ plays the role of a scale parameter and can replace N as a measure of the size of the system. A weaker (necessary but not sufficient) condition for Δ scaling is that the variance of the distribution should scale with its mean value as

$$\sigma^2 \sim \langle m \rangle^{2\Delta} \quad (2)$$

so that in a log-log plot of σ^2 versus $\langle m \rangle^2$ data should fall on a straight line of slope Δ .

The scaling law (1) with $\Delta = 1/2$ is associated with low-temperature (“ordered”) systems, or with observables that are not related to an order parameter. Scaling with $\Delta = 1$ is seen at high temperature (“disordered” system) and also for critical systems. For m to be an order parameter it must exhibit a corresponding change of Δ -scaling regime when some suitable control parameter (e.g., available energy, temperature, or bond-breaking probability) is varied.

Here it is worth saying a word about the comparison of experimental distributions using Eq. (1) and the determination of Δ -scaling regimes for data. As the transformation from experimental observable to the scaling variable $z_{(\Delta)}$ is a linear transformation, the form of the $\Phi(z_{(\Delta)})$ distribution is the same as that of $P_N[m]$. However, the presence of the exponent Δ in the scale factor $\langle m \rangle^\Delta$ means that two identical distributions will appear different (their widths will be different) if they are scaled using a value of Δ that is not the one relating the mean values and variances of the two distributions via Eq. (2). For example, consider two Gaussian distributions whose widths and mean values are related via Eq. (2) with $\Delta = 1$. In this case the use of Eq. (1) with, for example, $\Delta = 1/2$ would not lead to a universal scaling function: The widths of the two scaled distributions would be different, and, because of the normalization of $\Phi(z_{(\Delta)})$, the height of the distributions would differ also. It should also be noted that the relationship between the mean and the variance of a set of distributions, that is, the value of Δ if Eq. (2) holds, is quite independent of the form of the distributions: A given value of Δ does not imply a certain type of distribution, and vice versa.

More detailed information on the state of the system and the fragmentation process may be found in the form of the scaling functions $\Phi(z_{(\Delta)})$, Eq. (1). For systems far from a critical point, the central limit theorem tells us that for an observable m being the sum of uncorrelated random variables, one should observe asymptotically a Gaussian distribution for fluctuations of m about its mean value. If, however, m is an extremal value such as the largest among a set of uncorrelated random variables, then asymptotically its distribution should be that of Gumbel’s first asymptote [45]. For critical systems such general results do not exist, because the presence of correlations at all length scales means that the order parameter distribution must depend on the precise details of the interaction in this case. An asymptotic form of the large- m scaling function tail was derived in [42], where close to a critical point the order parameter distribution was expected to fall off like $\exp(-m^{\hat{\nu}})$ with $3 \leq \hat{\nu} \leq 6$, meaning that large deviations of the order parameter from its mean value are strongly suppressed.

There are two generic families of fragment production scenarios for which the second-order phase transition has been identified, with two different order parameters. These are as follows:

- the fragment multiplicity for *fragmentation scenarios* such as the fragmentation-inactivation binary (FIB) model [46] and
- the size of the largest cluster or fragment in *aggregation scenarios* such as percolation or Fisher droplet models [42].

Therefore the elimination of one of these two easily measurable experimental quantities as not having the order parameter Δ -scaling behavior described here should give important information on the fragment production process, by allowing us to exclude one of the two scenarios.

III. PRESENTATION OF DATA

A. Experimental details

To study as exhaustively as possible the question of the existence of an order parameter or other “phaselike” behavior in heavy-ion collisions, we have profited from the wide range of very high quality data that have been obtained with the INDRA 4π array [47–49] at the GANIL (Caen) and GSI (Darmstadt) accelerator facilities. This charged-product detector covers about 90% of the 4π solid angle. The total number of detection cells is 336 arranged according to 17 rings centered on the beam axis. The first ring (2° – 3°) was composed of 12 fast NE102/NE115 phoswich detectors during experiments at the GANIL facility. For the GSI experiments these were replaced by 12 telescopes composed of a $300\text{-}\mu\text{m}$ -thick silicon detector and a 14-cm-thick CsI(Tl) scintillator. Rings 2–9 cover the angular range from 3° to 45° and are made of three detector layers: a low-pressure gas-ionization chamber (5 cm of C_3F_8 at 20–50 mbar, depending on the experiment and the polar angle), a $300\text{-}\mu\text{m}$ -thick silicon detector, and a 14- to 10-cm-thick CsI(Tl) scintillator. The remaining eight rings cover the angular range from 45° to 176° and have two detection layers: an ionization chamber and a 7.6- to 5-cm-thick CsI(Tl) scintillator. Fragments with Z up to the charge of the projectile are identified with unit resolution in the forward region, when they are stopped in the scintillator detectors. Beyond 45° , the charge resolution is one unit up to $Z = 16$, and a few charges for larger Z . Over the entire angular range, very good isotope identification is obtained for $Z = 1$ to $Z = 3$, except for particles with low energies where ambiguities are unresolved.

The energy calibration of the CsI(Tl) scintillators was obtained for light charged particles (LCP) by means of the elastic and inelastic scattering of secondary LCP beams (p , d , t , ^3He , ^4He) produced by the fragmentation of a $95\text{A MeV } ^{16}\text{O}$ beam in a thick C target. These particles were then momentum selected by the “alpha magnetic spectrometer” of GANIL and scattered in a C or Ta target installed in the INDRA reaction chamber. A typical energy resolution was about 4%. Typical identification thresholds are a few 100 keV for light particles, 0.7A MeV for $Z = 3$, and 1.4A MeV for $Z = 35$. A complete technical description of INDRA, its calibration, and its electronics can be found in [47–53].

B. Overview of data

The data presented here cover a wide range of quasi-symmetric systems studied with the INDRA array, with different total masses and bombarding energies. They are as follows:

Ar + KCl: 32A, 40A, 52A, and 74A MeV;
Ni + Ni: 32A, 40A, 52A, 63A, 74A, 82A, and 90A MeV;

Xe + Sn: 25A, 32A, 39A, 45A, 50A, 65*A, 80*A, and 100*A MeV; and

Au + Au: 40*A, 60*A, and 80*A MeV.

The systems marked with an asterisk were measured during the experimental campaign at the GSI facility. We have concentrated on symmetric colliding systems to benefit from the maximum overall efficiency of the INDRA array in this case. Before presenting the analysis of this data set in terms of universal fluctuations we will give an overview of the chief characteristics of these reactions.

Figure 1 shows experimental data for the Xe + Sn system. The contour plots show the number of events measured corresponding to each value of the size of the largest detected fragment, Z_{max} , and of the fraction of the available energy converted into transverse energy of light charged particles, E_{t12}/E_{avail} . This latter quantity has been shown [29,31,54,55] to be principally related to the geometry of heavy-ion collisions in this energy domain and is particularly well suited to sorting events measured with the INDRA detector with little bias, because the efficiency of the array for light charged particle detection is $\approx 90\%$ whatever the centrality or reaction mechanism. The data shown were recorded with an online trigger requiring that at least four detectors fired in coincidence, whereas in the offline analysis we required at least four correctly identified charged products in each considered event. Very similar plots were obtained for all other data studied in this paper, as for example the data for the Ni + Ni system shown in Fig. 2. These give an overview of the evolution of reaction mechanisms with beam energy and impact parameter.

For the least violent collisions (small E_{t12}/E_{avail}) two strong contributions to the total cross section are observed, depending on whether the projectile-like fragment was detected ($Z_{\text{max}} \approx Z_{\text{proj}}$) or not ($Z_{\text{max}} < 10$). For most of these collisions the target-like residue is too slow-moving to be detected and/or correctly identified by the INDRA array. With increasing beam energy, the contribution from projectile-like fragments appears to decrease in importance. This is due to the increasingly forward-focused kinematics of the reactions and the smaller grazing angle at higher energy, which mean that projectile-like fragments from peripheral collisions are more likely to be deflected to angles too small for them to be detected in the first ring of the INDRA array (see Sec. III A).

For more central collisions (larger E_{t12}/E_{avail}) the outcome of the reaction depends on bombarding energy and the mass of the colliding nuclei. For the Xe + Sn system at the lowest incident energies [Figs. 1(a) and 1(b)], the cross section for all but the most peripheral collisions is dominated by events for which the heaviest detected fragment has around one-half of the charge of the projectile nucleus, and there is a discontinuous evolution in cross section between the most peripheral collisions and these events. This is due to the onset of fission of projectile-like nuclei above a certain threshold excitation energy, which is attained in mid-peripheral and more central reactions [55]. At higher bombarding energies [Figs. 1(c) and 1(d)], a more continuous evolution of projectile-like residue size with the collision violence is seen. For a lighter system such as Ni + Ni [Figs. 2(a) and 2(b)], a continuous ridge goes from the most peripheral toward more central collisions,

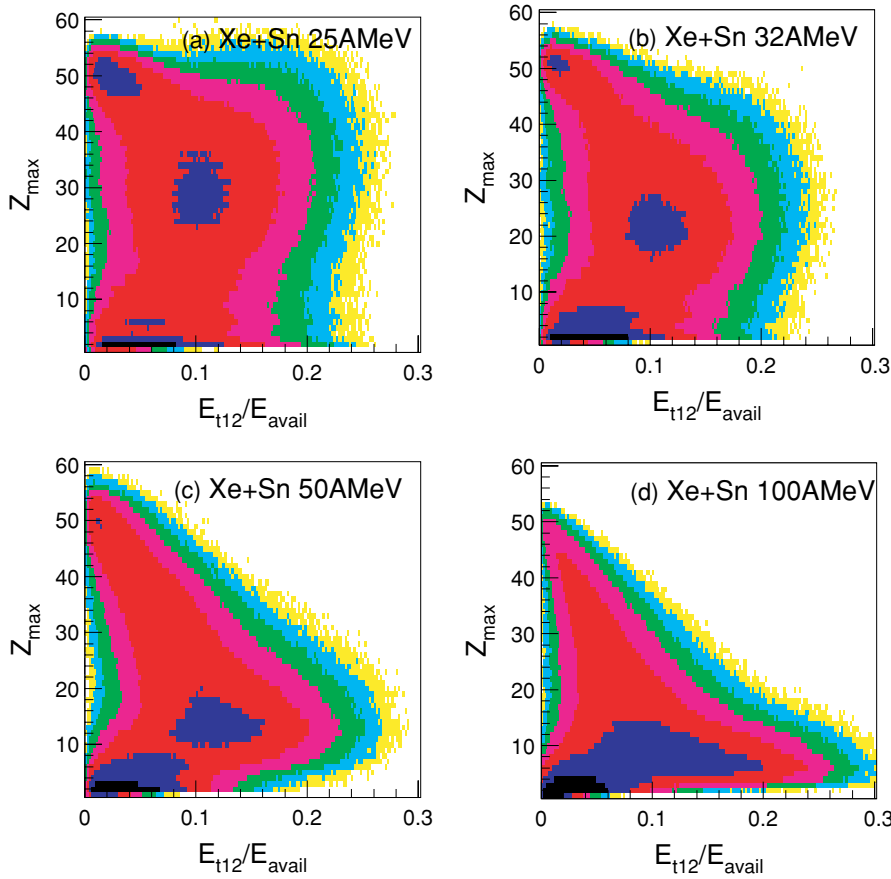


FIG. 1. (Color online) Experimental correlations between the size of the largest detected fragment Z_{\max} and the total transverse energy of light charged particles divided by the available c.m. energy, for Xe + Sn collisions. A minimum of four well-identified charged particles was required in the offline analysis. Logarithmic contour levels are shown corresponding to the number of events (with darker tones indicating larger numbers).

showing that the size of the projectile-like residues decrease continuously with decreasing impact parameter, as fission is not a predominant decay channel even at high excitation energies for such light nuclei. The correlations between Z_{\max} and E_{t12}/E_{avail} for the Ar + KCl system (not shown) are very similar to those for Ni + Ni, whereas for the Au + Au system they resemble those for Xe + Sn at 50A and 100A MeV except that for the most peripheral collisions a clear contribution from the fission of gold quasi-projectiles is seen.

Finally note the similarity between Figs. 1(a) and 2(a) concerning the production of heavy residues at low incident energy. Both figures show that there are two distinct contributions to the total yield for residues with Z close to that of the projectile. The first was discussed in the previous paragraph and is due to projectile-like fragments produced in peripheral collisions (small E_{t12}/E_{avail} values). This is the dominant contribution. Nevertheless, there is a second contribution associated with a broad distribution of large residue sizes $Z_{\text{proj}}/2 < Z_{\max} \lesssim Z_{\text{proj}}$ as well as an equally broad distribution of E_{t12}/E_{avail} values corresponding to mid-to central collisions. The appearance of these experimental correlations suggests that the mean value of the charge of the heaviest detected fragment, $\langle Z_{\max} \rangle$, first decreases with increasing collision violence and then increases for the most “central” collisions at the lowest beam energy for these two systems.

According to Figs. 1 and 2, such reactions make a relatively important contribution to the production of heavy residues in

central collisions of Ni + Ni and Xe + Sn at 32A and 25A MeV, respectively. When the incident energy increases [40A MeV for Ni + Ni, Fig. 2(b), and 32A MeV for Xe + Sn, Fig. 1(b)], the size and yield of the associated residues decrease, making this contribution harder to distinguish. From Figs. 2(c) and 2(d) and Figs. 1(c) and 1(d) it appears that the cross sections associated with these reactions become very small above $\sim 40A$ MeV, for the Ni + Ni system, or above $\sim 32A$ MeV, for the Xe + Sn system. (For the Ar + KCl system, not shown here, this contribution is discernible up to 52A MeV.) However, more sensitive analyses can reveal the survival of such reactions at higher incident energies.

Figure 3 shows the evolution of $\langle Z_{\max} \rangle$ with three different centrality selectors, for Xe + Sn collisions between 25A and 50A MeV: the total transverse energy of light charged particles, E_{t12} ; the total transverse energy of all charged products, E_t ; and the total multiplicity of charged products, N_C . Only well-measured events are considered, for which the ratio of the total detected charge to the total charge of projectile and target is at least 80%, ensuring that the largest fragment of the event is correctly identified. For each selector, $\langle Z_{\max} \rangle$ first decreases with increasing violence of the collision (smallest values of the selector variable). As previously mentioned, for these collisions $\langle Z_{\max} \rangle$ reflects the size of projectile- or target-like residues. With E_{t12} [Fig. 3(a)], $\langle Z_{\max} \rangle$ increases in central collisions at 25A and 32A MeV, whereas at 39A MeV and above it reaches a minimum value at which it saturates. With N_C [Fig. 3(c)] the same increase of $\langle Z_{\max} \rangle$ in central

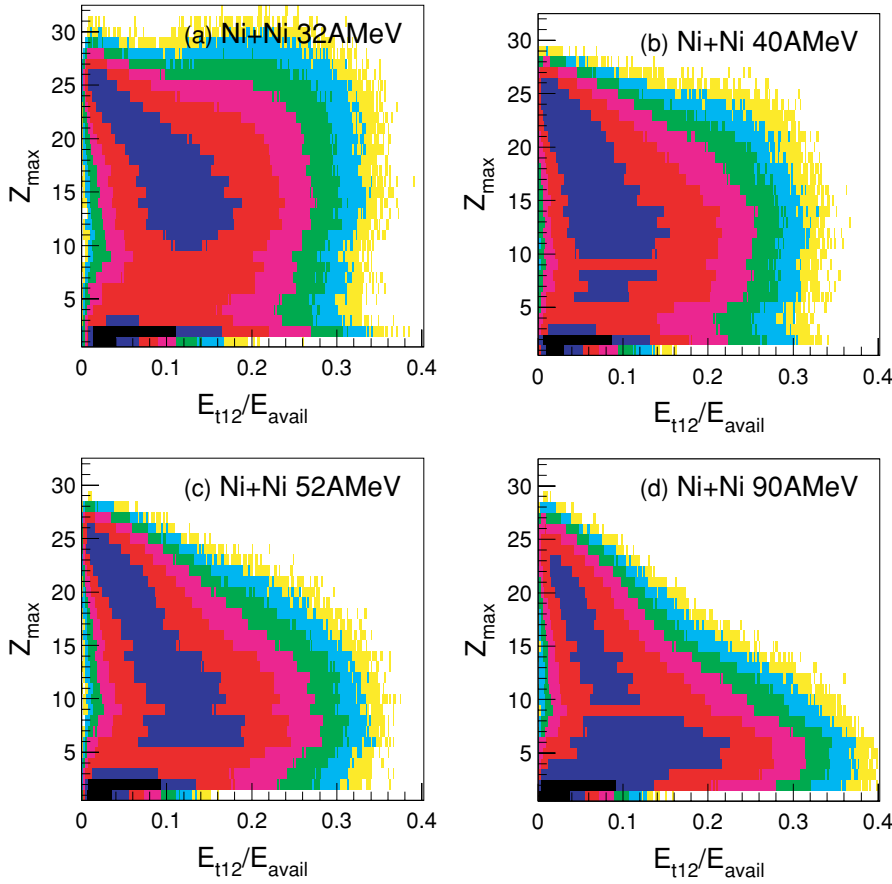


FIG. 2. (Color online) Experimental correlations between the size of the largest detected fragment Z_{\max} and the total transverse energy of light charged particles divided by available c.m. energy, for Ni + Ni collisions. A minimum of four well-identified charged particles was required in the offline analysis. Logarithmic contour levels are shown corresponding to the number of events (with darker tones indicating larger numbers).

collisions occurs at 25A MeV, whereas for 32A MeV and above it shows a decreasing trend for all values of N_C . The increase of $\langle Z_{\max} \rangle$ for central collisions suggests an important mass transfer between projectile and target at 25A MeV and, perhaps, at 32A MeV. This is clearly seen with E_{t12} and N_C . However, for E_t an increase is seen for all bombarding energies [Fig. 3(b)], but only for bins with large statistical errors. This effect is probably due to an autocorrelation between the selector and the observable. The contribution of the largest fragment to the transverse energy E_t is quite large, whereas its contribution to the total multiplicity N_C (which is also autocorrelated with the size of the largest fragment) is 1. This can explain why the evolution of $\langle Z_{\max} \rangle$ with E_t shows clear autocorrelation effects, whereas the evolution of $\langle Z_{\max} \rangle$ with N_C is qualitatively the same as that observed for the uncorrelated selector E_{t12} . Meanwhile, the larger dynamic of the E_{t12} variable offers the possibility of greater sensitivity in event selection than the (integer) variable N_C .

In Fig. 4 we can follow the correlated evolution of the variance and the mean of the Z_{\max} distribution as a function of collision violence: from peripheral collisions leading to a slightly excited quasi-projectile (large $\langle Z_{\max} \rangle$ and small variance) to the most central collisions (indicated by a ring around the last data point for each beam energy). To do this we considered only events for which at least 75% of the momentum of the incident beam particles is reconstructed from the detected nuclei. In this way we retain all events for

which at least a good reconstruction of the quasi-projectile residue and products was obtained, in the most peripheral collisions, while in the most central collisions we achieve an almost complete reconstruction of the event. Each point in this figure corresponds to E_{t12} cuts defined by slicing the minimum-bias distribution into 100 bins, each containing an equal number of events. Thus each point represents 1% of the measured cross section, although owing to our requirement of well-measured events the most peripheral (least well measured) events are absent. This allows us to see how in the most central collisions two different behaviors are observed depending on the incident beam energy: Below 39A MeV in the 3–5% most central collisions the mean charge of the largest fragment actually begins to increase again, whereas the correlation between this mean value and the variance of the distribution is not the same as for the majority of other impact parameters.

This figure suggests that at beam energies $\lesssim 39$ A MeV the origin of the heaviest fragment is not the same in central collisions as for the rest of the reactions. The increase of $\langle Z_{\max} \rangle$ for the most central collisions at these energies suggests a contribution from (incomplete) fusion reactions where the heaviest fragment detected is an evaporation residue. The disappearance of this phenomenon for $\gtrsim 39$ A MeV can be interpreted as signaling the onset either of fusion-evaporation residues and marking the onset of fusion multifragmentation [34] or of transparency in central collisions (incomplete stopping) [30,56,57].

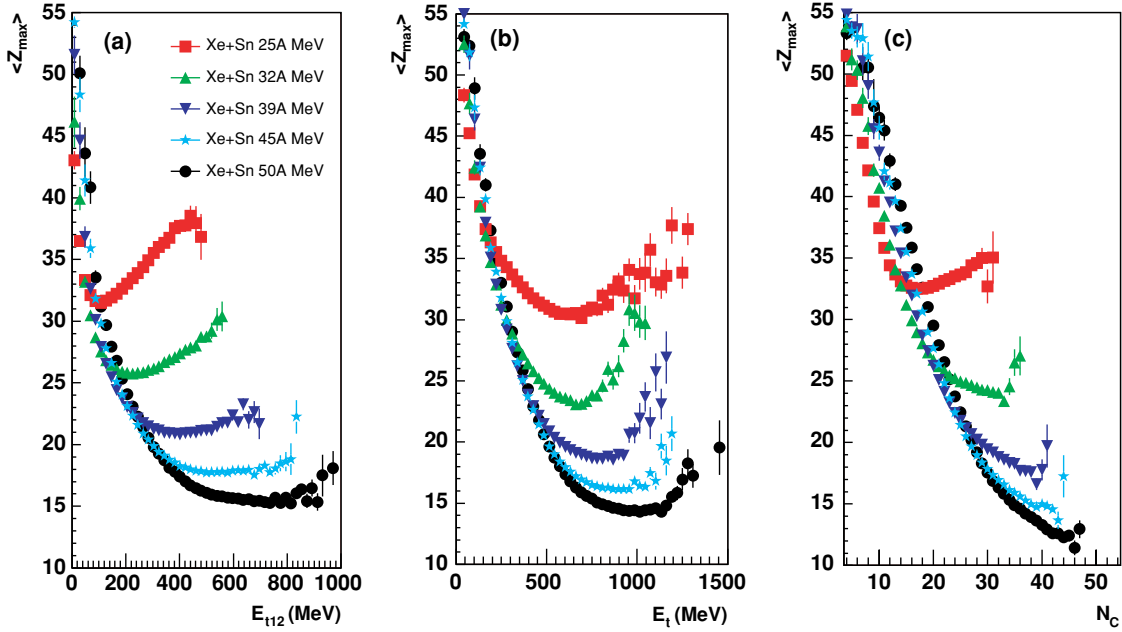


FIG. 3. (Color online) The mean charge of the largest fragment detected in each event, Z_{\max} , as a function of (a) the total transverse energy of light charged particles, E_{t12} ; (b) the total transverse energy of all charged particles and fragments, E_t ; and (c) the total multiplicity of charged products, N_c . Vertical bars show the statistical error on the mean value for each bin. To retain only the most significant data, bins to which fewer than 10 events contributed were excluded from the plots.

IV. ANALYSIS OF DATA IN TERMS OF UNIVERSAL FLUCTUATIONS

A. Selection of central collisions

We begin our analysis by extending the results of [44], for central collisions of Xe + Sn, to a wider range of systems measured with the INDRA multidetector array. As was discussed in Sec. I, the analysis of universal fluctuations in multifragmentation data does not require knowledge (or supposition) of how fragments are formed. However, the comparison of events with very different collision geometries

is unlikely to give meaningful results. Therefore we will limit our study to very central collisions for which the geometrical overlap between projectile and target is as close as possible to total. The need to select equivalent classes of events for a large range of system masses and beam energies with as little dependence as possible on detector efficiency led us to use the total transverse energy of light charged particles, E_{t12} .

The sorting variable E_{t12} has been studied specifically for the INDRA detector. It was shown that, for a given projectile-target system, the minimum-bias inclusive distributions of E_{t12}

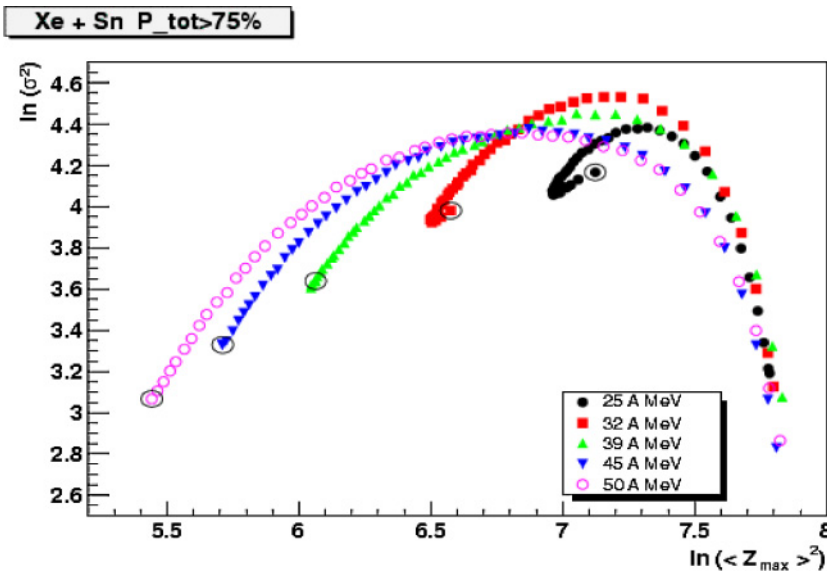


FIG. 4. (Color online) Collisions from the most peripheral with detection of a quasi-projectile residue (furthest right-hand side of the figure) to the most central (indicated by a ring) sorted into bins corresponding to 1% of the total measured cross section.

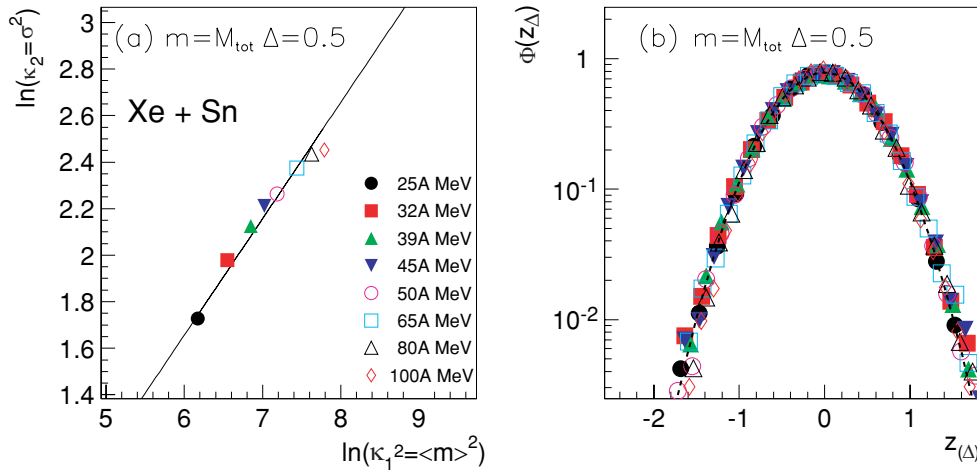


FIG. 5. (Color online) Data for the total multiplicity of charged products with $Z \geq 1$, M_{tot} , for well-measured central collisions of Xe + Sn [$b < 0.1b_{\text{max}}$, $Z_{\text{det}} \geq 0.8(Z_{\text{proj}} + Z_{\text{targ}})$]. (a) Log-log plot of the variance versus the squared mean value of the distribution of M_{tot} for each bombarding energy. The straight line represents Eq. (2) with $\Delta = 1/2$. (b) Experimental distributions of M_{tot} expressed in the variables of the second scaling law, that is, Eq. (1) with $\Delta = 1/2$. The dashed curve is a Gaussian fit to all the data.

for different beam energies scale as a function of the available center of mass energy [31,58], consistent with E_{t12} being mainly sensitive to the geometry of the collisions, that is, that it is a good indicator of collision centrality. Moreover, as it was pointed out in Sec. III B, the efficiency of the INDRA detector for light charged particles is almost independent of the type of reaction under study, allowing us to use this variable to sort all data considered in this paper in the same way. It should be noted that the total transverse energy of all charged products (including the heaviest), E_t , does not exhibit any scaling with beam energy for our data, probably because of the variable efficiency of the INDRA array for heavy fragment detection as a function of impact parameter. Therefore, although one may expect E_t to contain more information on the events than a variable limited to the kinematical properties of only $Z = 1, 2$ particles, the specificities of INDRA data make E_{t12} a more suitable selector.

In addition, by using E_{t12} we avoid any direct link between the studied observables (size of the largest fragment in each event and fragment multiplicity) and the variable used for the selection of events. We are therefore in the best possible situation to avoid distortion of the data caused by autocorrelations with the experimental filter [15].

The data analyzed in the following with the largest values of E_{t12} correspond to 1% of the total number of events recorded during the experiment with a minimum-bias condition ($b < 0.1b_{\text{max}}$ in the geometrical approximation of [59], where the maximum impact parameter b_{max} is smaller than the sum of the radii of projectile and target due to the experimental trigger condition). We were able to check whether the largest detected charged fragment of each event is really the largest, using the total detected charge of the event, Z_{tot} .

B. Establishing an “order parameter” for nuclear multifragmentation with no model-dependent hypotheses

Generic models of cluster production may be classed into two types. The first, the class of “fragmentation” scenarios in

which a system is broken up by a series of binary splittings or some other physical process, has for its order parameter the number or multiplicity of clusters. For such models, it is the multiplicity that exhibits different Δ -scaling regimes if the system has different phases. The second class of models, in which clusters are built up by “aggregation” of smaller constituents, has for its order parameter the size of the largest cluster. As INDRA does not measure the mass but only the atomic number of fragments, we will assume in the following that the largest fragment of each event corresponds to Z_{max} , the fragment with the largest atomic number.

Figure 5 shows the data for the total multiplicity of charged products with $Z \geq 1$, M_{tot} , for central collisions of Xe + Sn from 25A to 100A MeV. In Fig. 5(a) we plot the natural logarithm of the variance of the measured M_{tot} distributions as a function of the natural logarithm of the square of the mean value. The estimated statistical errors of these quantities are smaller than the symbols used. If fluctuations obey the universal scaling law [Eq. (2)], then the data must fall on a straight line of slope Δ in this plot. It can be seen in Fig. 5(a) that this is true to a fair approximation and that the variance of the multiplicity distribution grows with increasing bombarding energy as $\langle M_{\text{tot}} \rangle$.

Figure 5(b) shows that the multiplicity distributions for different bombarding energies collapse to a unique distribution (scaling function) when expressed in terms of the second scaling law [Eq. (1) with $\Delta = 1/2$], as suggested by Fig. 5(a). It should be noted that examination of an observable’s scaling properties in this way is far more constraining than that of Fig. 5(a), when the statistics of the data samples allow it. The observed scaling function is very well approximated by a Gaussian distribution (dashed curve on the figure). The scaling properties of total multiplicity fluctuations are therefore the same for all bombarding energies in the range 25A–100A MeV. This is true not only for the Xe + Sn data but also for all the data we have studied in this paper [see, for example, the data for $^{58}\text{Ni} + ^{58}\text{Ni}$ collisions in Fig. 6(a)].

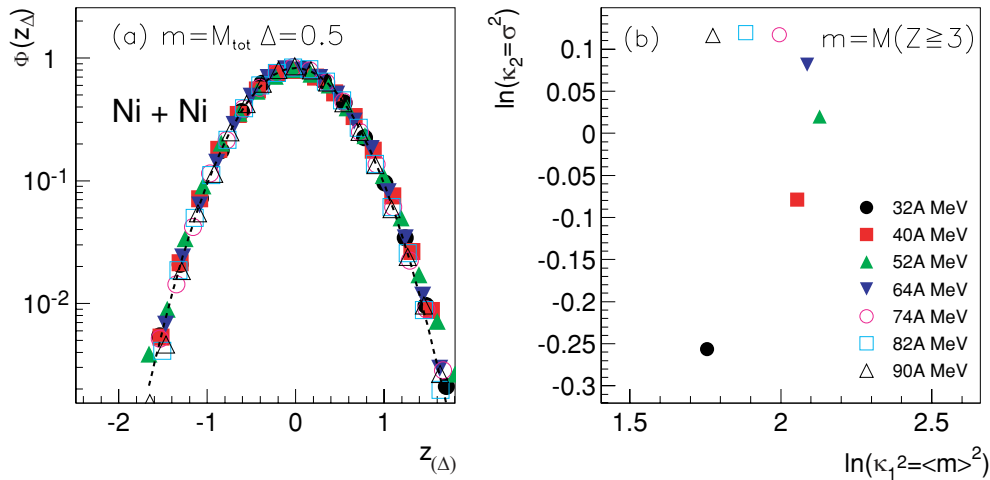


FIG. 6. (Color online) Data for well-measured central collisions of Ni + Ni [$b < 0.1b_{max}$, $Z_{det} > 0.8(Z_{proj} + Z_{targ})$]. (a) Distributions of M_{tot} expressed in the variables of the second scaling law, that is, Eq. (1) with $\Delta = 1/2$. The dashed curve refers to a global Gaussian fit to the data. (b) Log-log plot of the variance versus the squared mean value of the distribution of fragment multiplicity $M_{Z \geq 3}$ for each bombarding energy.

Therefore the total multiplicity of charged particles for central collisions in this energy range does not show any evidence of “anomalous” or “critical” behavior.

The multiplicity M_{tot} is dominated by the multiplicity of light charged particles, M_{LCP} , which is typically 3–4 times greater than the multiplicity of IMF ($Z \geq 3$). However, similar conclusions as for M_{tot} can be drawn for the IMF multiplicity, $M_{Z \geq 3}$, for which the Xe + Sn data are presented in Fig. 7 and the Ni + Ni data in Fig. 6(b). Figure 7(a) shows that the widths of $M_{Z \geq 3}$ distributions for Xe + Sn at bombarding energies of 32A to 65A MeV increase with the mean multiplicity according to a $\Delta = 1/2$ scaling law, and this is confirmed by Fig. 7(b). The width for the 25A MeV system falls below this “systematic” trend, which may indicate that this energy is close to the threshold for multifragmentation in central collisions (with a mean multiplicity for this system of approximately 3

fragments with $Z \geq 3$), leading to reduced fluctuations of the fragment multiplicity. Recent data obtained with INDRA for the same system at bombarding energies from 8A to 20A MeV will allow us to study this point in more detail.

Nevertheless, the multiplicity of fragments does show some slightly more interesting features than M_{tot} . Note the “back-bending” in Fig. 7(a) for bombarding energies $> 65A$ MeV, indicating a decrease of mean fragment multiplicity at the highest bombarding energies. The same behavior is seen more clearly in Fig. 6(b) for Ni + Ni collisions above 52A MeV. Let us note in passing that the available energy for the maximum of fragment production in the Ni + Ni system is here much lower (13A MeV) than that reported in [60] (17.5A MeV).

This type of “rise and fall” behavior has been observed in many different data sets [3–5,60]. The absolute value of the maximum mean multiplicity and the energy at which it occurs

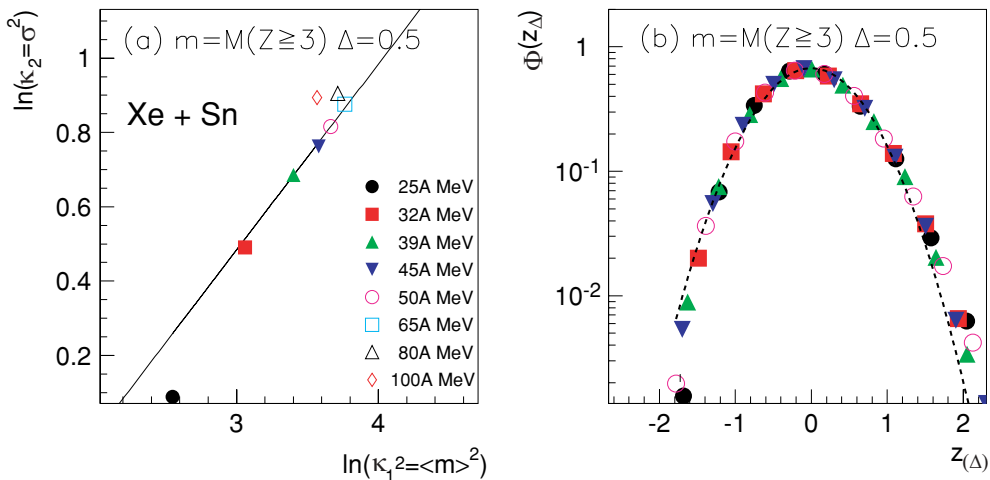


FIG. 7. (Color online) Same as Fig. 5 but now for the multiplicity of fragments with $Z \geq 3$, $M_{Z \geq 3}$. (b) Data for bombarding energies 32A–65A MeV expressed in the variables of the second scaling law, that is, Eq. (1) with $\Delta = 1/2$.

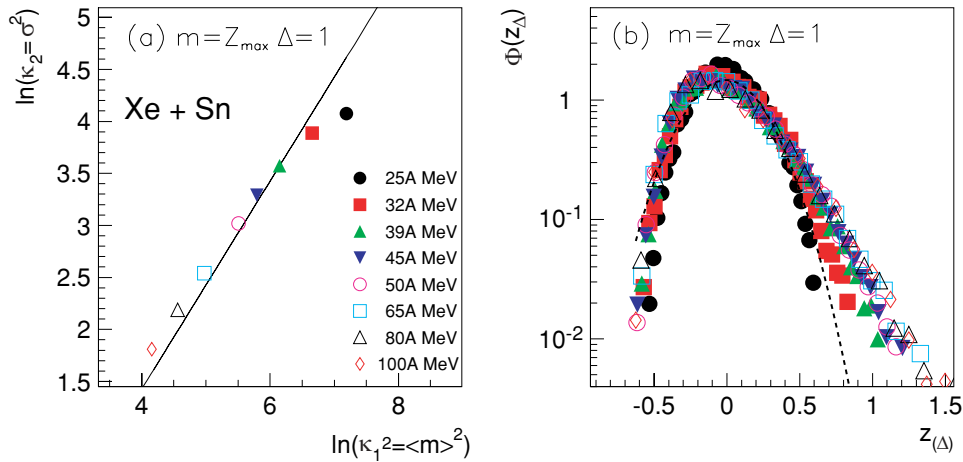


FIG. 8. (Color online) Same as Fig. 5 (well-measured central Xe + Sn collisions) but for the charge Z_{\max} of the heaviest fragment detected event-by-event, and with $\Delta = 1$.

in central collisions are not only system dependent [60] but also selection dependent [15] and detector dependent. It should be noted that in the framework of the universal fluctuations theory this rise and fall is not consistent with the fragment multiplicity being an order parameter. Rather, in the energy domain for which fluctuations of $M_{Z \geq 3}$ show a regular scaling behavior (32A–65A MeV for Xe + Sn), it can be seen that this scaling is always of the second kind ($\Delta = 1/2$) and in this domain the multiplicity distributions all collapse to a unique, quasi-Gaussian scaling function [Fig. 7(b)].

Therefore, neither the total charged multiplicity nor the fragment multiplicity have fluctuations that indicate the presence of different “phases” for central collisions in this energy range. It should be noted, however, that we cannot exclude the possibility of a different behavior of observables to which we do not have access in those data, for example the true total multiplicity including neutrons. Nor does our result exclude the possibility that in other fragmentation reactions (e.g., at higher bombarding energies and/or in spectator decays rather than central collisions) the total or fragment multiplicity may be the pertinent order parameter. For our data on central collisions between 25A and 100A MeV, however, we will from now on only consider the other possible order parameter for fragmentation, the size of the largest fragment.

Looking at the log-log plot of the first two cumulant moments of Z_{\max} [Fig. 8(a)] we can suspect some evolution of the scaling behavior of this observable’s fluctuations with increasing beam energy: The data do not appear to fall on a single straight line, but rather they seem to be grouped into two “branches” with different slopes. Although most of the data in Fig. 8(a) lie close to a line of slope $\Delta = 1$, this does not correspond to a universal scaling law, as all data in Fig. 8(b) do not collapse onto a single universal curve under the first scaling law [Eq. (1) with $\Delta = 1$]. This confirms that there is a change in the scaling behavior of Z_{\max} fluctuations with increasing energy. The charge of the largest fragment in each event, and not the fragment multiplicity, seems therefore to be a good candidate for the order parameter of multifragmentation in central collisions at these energies.

C. Evolution of the scaling behavior of order parameter fluctuations with incident energy

Figure 8(b) shows that the scaled Z_{\max} distributions for Xe + Sn collisions from 45A MeV upward are nearly identical even in the large- Z_{\max} tails, which are two orders of magnitude less probable than the most probable value of Z_{\max} . The 39A MeV data can also be included in this group if the small differences in the tail of the distribution are neglected. However, the 32A MeV distribution is clearly significantly narrower, whereas the distribution for 25A MeV is evidently of a different form, as can be seen both in the tails and around the maximum (see comments on the comparison of experimental distributions with this technique in Sec. II).

Using the values of Δ extracted from Fig. 8(a) using a linear fit to the two “branches” (25A–39A MeV and 39A–100A MeV) we find a good scaling of distributions using $\sigma \sim \langle Z_{\max} \rangle^{1/2}$ at the lowest beam energies [Fig. 9(a)], whereas for the higher energies the fluctuations of the size of the largest fragment increase like $\sigma \sim \langle Z_{\max} \rangle$ [Fig. 9(b)]. An approximately equally good scaling for 39A MeV data is achieved in both cases, and this energy may be considered as close to a transition between the two regimes. Figure 9 also shows that the shape of the scaling function changes with increasing beam energy: It is nearly Gaussian at low energy [with the dashed curved in Fig. 9(a) representing a best fit to all data with a Gaussian distribution], but at higher energies it is rather asymmetric with a near-exponential tail for Z_{\max} greater than its most probable value (see Sec. IV E).

These observations establish the size (or charge) of the largest fragment as the most likely “order parameter” for fragment production in central collisions in this energy range. They also show that data can be assigned to one of two regimes depending on the Δ -scaling properties of this order parameter. At low energies systems obey the second-scaling law associated with an ordered phase, whereas at higher energies, the first-scaling law is observed, typical of a disordered phase (large fluctuations) [42]. It should be noted that these regimes are defined, not by the average size of the largest fragment

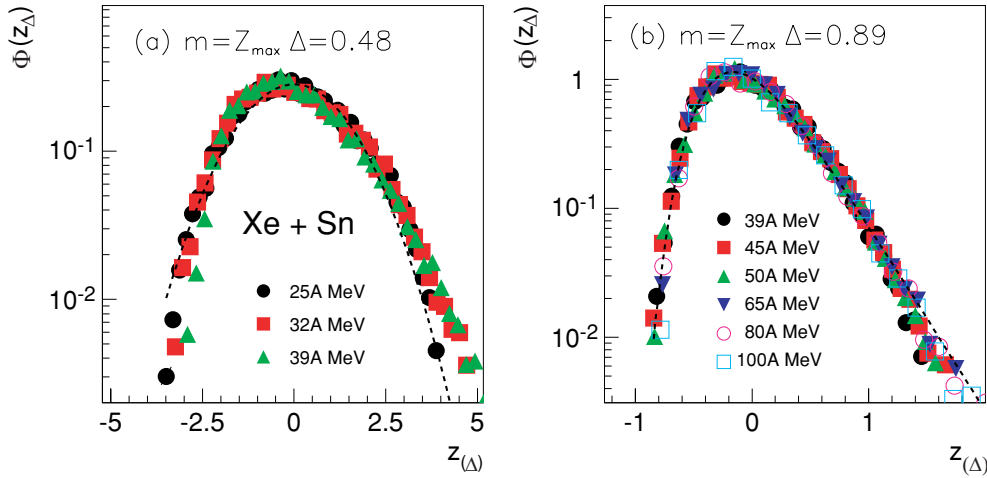


FIG. 9. (Color online) (a) Z_{\max} distributions for Xe + Sn collisions at 25A–39A MeV, scaled according to Eq. (1) with Δ given by a linear fit to the data of Fig. 8(a) of the form $\sigma \sim \langle m \rangle^\Delta$. The dashed curve is a best fit to scaled data using a Gaussian distribution. (b) Same as (a) but for bombarding energies 39A–100A MeV. The dashed curve is a best fit to scaled data using the Gumbel distribution, Eq. (5).

produced for a given incident energy (which would be a typical way to define, e.g., liquid and gas phases), but rather by the way in which the fluctuations of this quantity evolve compared to its mean value. The identification of the largest fragment size as order parameter also indicates some similarity between fragment production in central collisions and the aggregation models with the second-order phase transition mentioned in Sec. II, whereas the monotonic behavior of total and fragment multiplicities excludes “shattering” fragmentation models such as FIB [46].

Another, not necessarily incompatible, interpretation of the different Δ regimes is suggested by Fig. 4. As we remarked in Sec. III B, this figure suggests that at beam energies $\lesssim 39A$ MeV the heaviest fragment in central collisions is an evaporation residue of an incomplete fusion reaction. The data presented in Fig. 8(a) for incident energies 25A–50A MeV correspond to the points highlighted by a circle in Fig. 4. Therefore the transition from a $\Delta \sim 1/2$ to a $\Delta \sim 1$ branch can be interpreted as being linked to the disappearance of fusion-evaporation residues and signaling either the onset of fusion multifragmentation (phase transition) or the onset of transparency in central collisions (incomplete stopping).

It should be noted that the transition energy of around 39A MeV for the Xe + Sn system is slightly higher than that found in [44] (32A MeV). This is due to the different method of selection of “central collisions.” In this paper we define central collisions based on the amount of energy deposited into the light charged particles’ degrees of freedom (E_{l12}). As we are dealing with finite systems this reduces the energy available for the fragment degrees of freedom, owing to energy conservation. This is consistent with the fact that when central collisions are selected based on fragment degrees of freedom (the fragment kinetic energy flow angle selection of [28,34,61]) the multifragmentation regime is observed at lower incident energy for the same system (32A MeV for Xe + Sn in [35]), as is the transition to the $\Delta = 1$ scaling regime.

The observed scaling properties of Z_{\max} fluctuations are confirmed by the Ni + Ni data, as shown by Figs. 10 and 11.

Most data follow a $\Delta \approx 1$ scaling law for Z_{\max} fluctuations, except at the lowest energies. The data do not all collapse to a single scaling function in terms of a $\Delta = 1$ law [Fig. 10(b)], but only for bombarding energies $E \geq 52A$ MeV [Fig. 11(b)]. The similarity between the scaling functions observed for the two different systems should be noted, both in the “ordered” ($\Delta \sim 1/2$) and “disordered” ($\Delta \sim 1$) regimes (Figs. 9 and 11 and Table I).

D. System-size dependence of energy of transition from “ordered” to “disordered” regime

We observe for the Xe + Sn and Ni + Ni data that the energy ranges corresponding to the different regimes are not the same for two systems of different total mass, with the “transition” occurring around 39A MeV for Xe + Sn and 52A MeV for Ni + Ni. The “disordered” regime begins at lower incident (or available) energy for the heavier system. This tendency is confirmed by the data for Ar + KCl and Au + Au (Figs. 12 and 13). The former has a

TABLE I. Fluctuation scaling exponent Δ , coefficient of skewness γ , kurtosis κ , χ^2 for global fits to data with Gaussian ($\Delta \sim 1/2$) and Gumbel ($\Delta \sim 1$) distributions, and scaling function tail exponent $\hat{\nu}(\chi^2)$ (see Sec. II), for the scaling functions shown in Figs. 9 and 11–13.

System	E_{inc} (AMeV)	Δ	γ	κ	χ^2	$\hat{\nu}(\chi^2)$
Xe + Sn	25–39	0.48	0.45	0.66	27	—
Ni + Ni	32–52	0.61	0.48	0.64	72	—
Ar + KCl	32–52+	0.46	0.33	0.64	63	—
Au + Au	40–80	1.00	0.83	1.39	1.8	$0.92 \pm 0.09(1.3)$
Xe + Sn	39–100	0.89	0.85	1.20	11	$1.20 \pm 0.03(1.2)$
Ni + Ni	52–90	0.88	0.84	1.30	45	$1.54 \pm 0.04(7)$

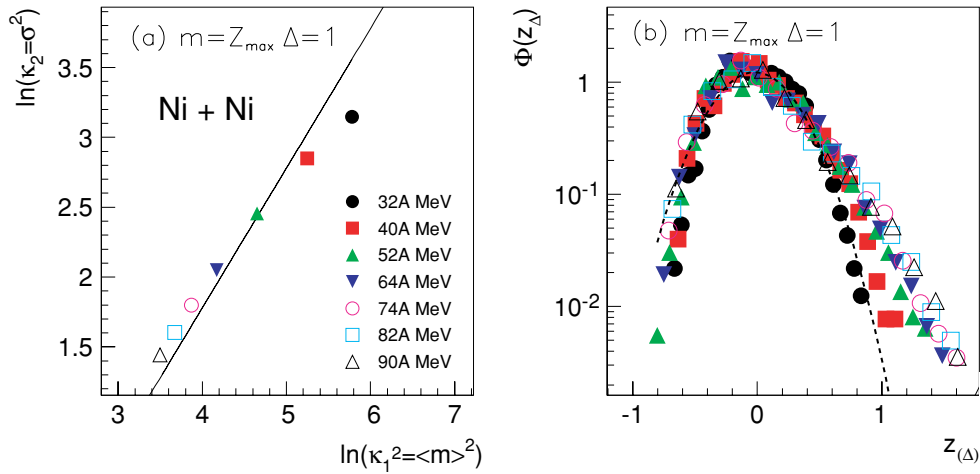


FIG. 10. (Color online) Same as Fig. 8 but for collisions of Ni + Ni from 32A to 90A MeV bombarding energy.

total mass smaller than both Xe + Sn and Ni + Ni. The largest fragments produced in central collisions of ³⁶Ar + KCl follow quite closely a $\Delta \sim 1/2$ scaling behavior for beam energies up to at least 52A MeV [Fig. 12(a)], whereas the data for 74A MeV, which deviate from the overall trend, may indicate a transition to the $\Delta \sim 1$ regime occurs somewhere between these last two available data points. The data for 32A–52A MeV exhibit very similar near-Gaussian probability distributions. Although we cannot have much confidence in a scaling law established for only two data points let us remark in passing that the scaling behavior observed for data at 52A and 74A MeV is approximately a $\Delta \sim 1$ scaling with a scaling function of a form similar to that observed for the other “disordered” regime data, indicating that the transition energy for this system is probably somewhere between 52A and 74A MeV, higher than for the heavier systems.

However, for the much heavier ¹⁹⁷Au + ¹⁹⁷Au system a $\Delta = 1$ scaling law is observed for fluctuations of the size of

the largest fragment in each event for all studied beam energies (Fig. 13). Even at the lowest energy (40A MeV) the scaling of the entire Z_{\max} distribution with the other energies is excellent. For this system it may be that the beam energy of the transition from the $\Delta = 1/2$ regime, if it exists, to $\Delta = 1$ occurs at a lower energy than the lowest energy available for study in our data, which may explain why we do not observe an “ordered” regime for this system. Of course it is equally possible that no such regime exists for this system. Indeed, following the interpretation of Sec. IV C in terms of the disappearance of fusion-evaporation residues, we would not expect fusion to occur for a system as heavy as Au + Au at any incident energy.

We therefore observe that the bombarding energy (or available energy) at which there is a transition from the “ordered” to the “disordered” regime decreases with increasing total mass of the system under study. This is represented in Fig. 14. If one interprets our results in the framework of universal fluctuations theory (i.e. in terms of a second-order

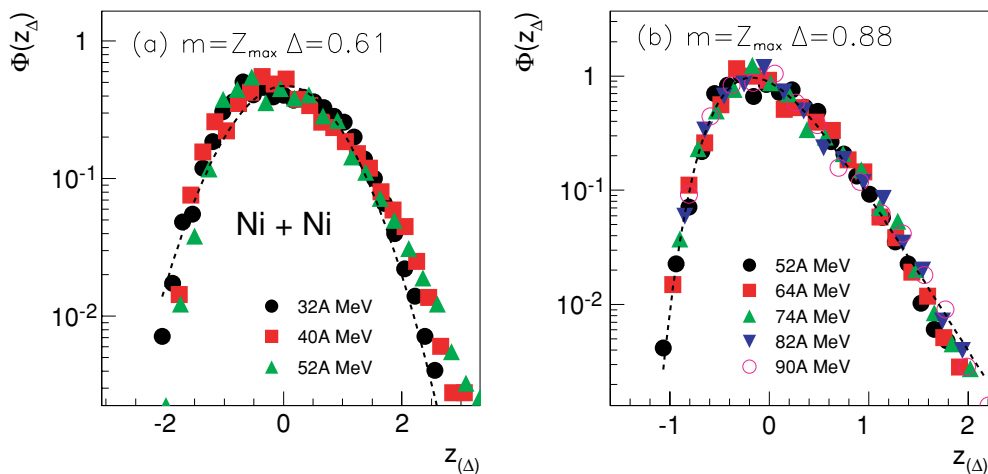


FIG. 11. (Color online) (a) Z_{\max} distributions for Ni + Ni collisions at 32A–52A MeV, scaled according to Eq. (1) with Δ given by a linear fit of the form $\sigma \sim \langle m \rangle^\Delta$. The dashed line is a best fit using a Gaussian distribution. (b) Same as (a) but for energies 52A–90A MeV. The dashed line is a best fit using the Gumbel distribution, Eq. (5).

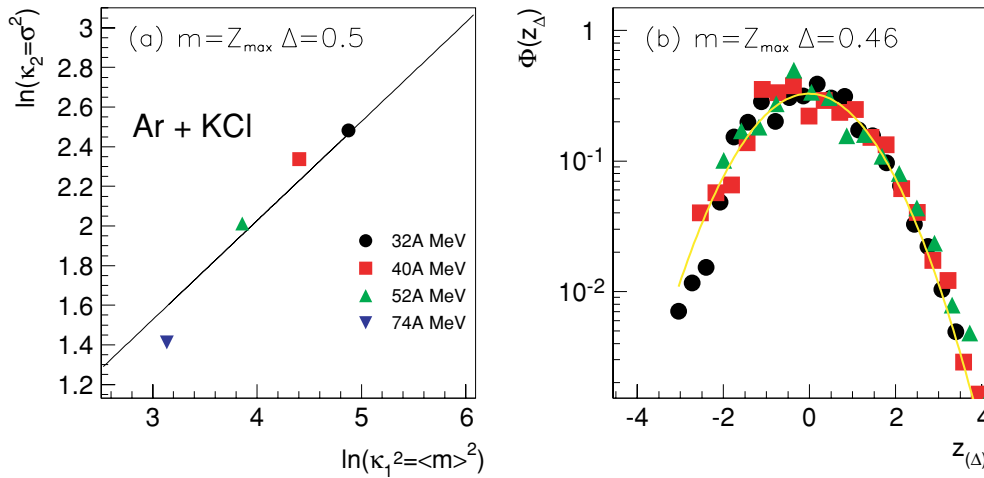


FIG. 12. (Color online) Same as Fig. 8 but for collisions of Ar + KCl from 32A to 74A MeV bombarding energy.

phase transition) one would expect the energy at which one phase is replaced by the other to be related to the critical temperature of the corresponding system. The definition of this quantity for finite, charged systems such as nuclei has received much theoretical attention. On the one hand, in the absence of Coulomb forces, we can define a pseudo-critical temperature (corresponding to a large peak in the finite system specific heat) that is smaller than the infinite matter value T_C and increases as the size of the system approaches the infinite matter limit [62]. On the other hand, calculations including the Coulomb repulsion show that the maximum temperature that an equilibrated hot nucleus can support, T_{lim} , decreases for heavier nuclei, owing to their increasing nuclear charge [63]. A recent systematic study of a wide range of data on so-called caloric curves by Natowitz *et al.* [64] has shown that the temperature and excitation energy at which a plateau is observed in these curves decrease with increasing mass of the primary excited nucleus and that such behavior is consistent with theoretical predictions for the limiting temperatures, T_{lim} .

In the present analysis we chose not to study this question in more detail, as to do so would require us to (i) show that

the fragment production is thermally driven, (ii) identify the thermal (sub)system in each case, and (iii) deduce the mass, charge, excitation energy, and temperature of this (sub)system. Each step would require us to make important hypotheses about the formation and decay properties of fragments in the collisions under study, taking us far from our initial goal of determining as much information as possible on the nature of fragment production with a minimum number of suppositions. Moreover, the observed effect, which depends on the entrance channel total mass and bombarding energy may have a completely different origin. Therefore we will limit ourselves to the observation that the transition from “ordered” to “disordered” regime takes place at a lower available energy for systems of greater total mass.

E. Detailed study of the form of the scaling functions

The results of the analysis for all the systems presented here are summarized in Table I. Systems have been grouped according to their observed Δ -scaling behavior, $\Delta \sim 1/2$ at the

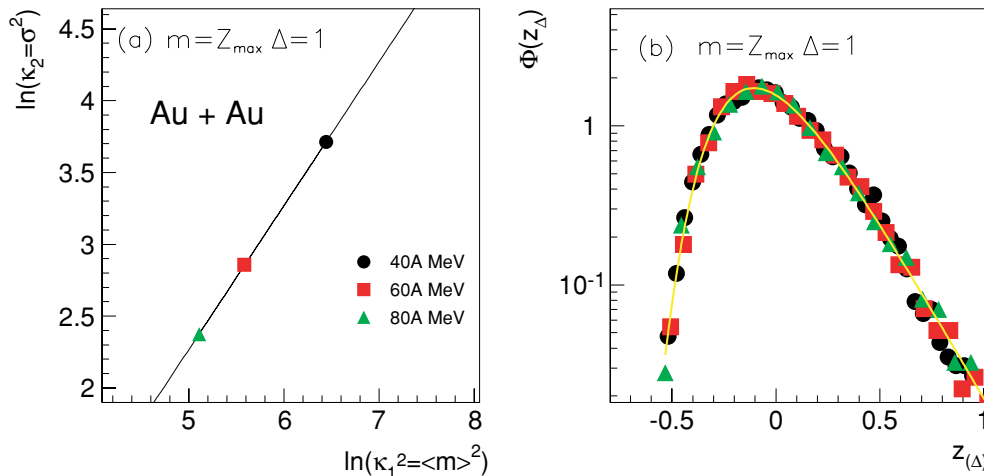


FIG. 13. (Color online) Same as Fig. 8 but for collisions of Au + Au from 40A to 80A MeV bombarding energy.

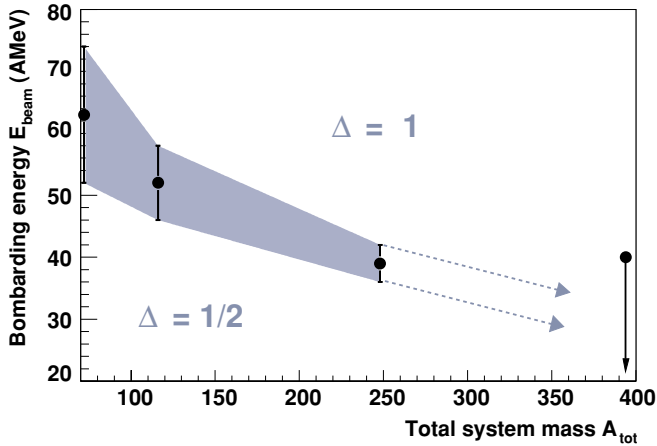


FIG. 14. (Color online) Dependence on bombarding energy and total system mass of the frontier between the two Δ -scaling regimes observed in this work for very central collisions.

lowest beam energies and $\Delta \sim 1$ at the highest. To get some quantitative information on the form of the scaling function in each case, we calculated the overall coefficient of skewness γ and the kurtosis κ for each system in each regime, using the following definitions [65]:

$$\gamma = \frac{\langle z_{(\Delta)}^3 \rangle}{\sigma^3} \quad (3)$$

and

$$\kappa = \frac{\langle z_{(\Delta)}^4 \rangle}{\sigma^4} - 3. \quad (4)$$

Larger skewness values indicate more asymmetric distributions, whereas the kurtosis measures the deviation of the distribution from the Gaussian form (with $\kappa = 0$ being a perfect Gaussian). The values shown in the table confirm our observation that the higher energy, $\Delta \sim 1$ scaling data present more asymmetric, less Gaussian probability distributions than those at lower energy. It can also be seen that, quantitatively, the scaling functions corresponding to the two regimes for systems of different masses have very similar forms, confirming the fact that data for different systems do indeed collapse onto a single distribution.

In the “ordered” regime the fluctuations of the size of the largest fragment show a significant deviation from a Gaussian distribution, contrasting with the near-perfect Gaussian distributions that we observe for total and fragment multiplicities (Figs. 5–7). For the “disordered” regime the deviation from the Gaussian form is large and the shape of the distribution function is well reproduced by a Gumbel distribution,

$$\Phi(z_{\Delta}) \sim \exp(-(z - e^{-z})). \quad (5)$$

This distribution is shown by the dashed curves in Figs. 9(b) and 11(b) and the gray curve in Fig. 13(b), which represent the best fits to these data using Eq. (5). The overall agreement can be seen to be quite good, and it is excellent for the Au + Au data where $\chi^2 = 1.8$ is achieved. Some significant deviations can be seen, however, in the tail of the distributions for the

lighter systems Ni + Ni and Xe + Sn: The data seem to have a faster-than-exponential falloff for large (positive) fluctuations about the mean value.

To confirm this in a quantitative manner we performed fits to the tails of these functions with the asymptotic scaling function form $\exp(-z^{\hat{\nu}})$ (see Table I). They show that the exponent $\hat{\nu}$ is very close to 1 for the Au + Au data, confirming the observation of an exponential tail compatible with the Gumbel distribution, whereas for Ni + Ni and Xe + Sn data we find $1 < \hat{\nu} < 2$. Let us remark in passing that, just as Δ seems to increase toward the asymptotic value of 1 with increasing system mass in the “disordered” regime, it is possible that $\hat{\nu}$ also has a systematic mass dependence and decreases toward an asymptotic value of 1 (exponential tail) for the heaviest system.

We have clearly and quantitatively established the form of the scaling functions in the two regimes, and in the data presented here we do not observe any deviation from these “canonical” forms, quasi-Gaussian at low energy and quasi-Gumbel at high energy. We do not, therefore, have any information on the nature of the transition between the two regimes: As we discussed in Sec. II we cannot be certain of the form of the scaling function at the critical point, but one may see a sharp decrease of the large- z tails [faster than $\exp(-z^2)$] or an order parameter distribution (OPD) with an exponential large- z tail but significantly different from the Gumbel distribution around the maximum and below [66]. However, for a first-order phase transition with a passage through the coexistence region, although the scaling behavior of the OPD is not well established [42,67], by definition in this case the order parameter should present a bimodal (double-humped or very wide) distribution. More detailed study of existing and new data around the transition energy of 394 MeV (for the Xe + Sn system) may yet reveal such features.

F. Dependence of the observed scaling behavior on the violence and centrality of collisions

The results we have presented come from a wide-ranging set of data concerning different system energies and masses, but they represent only 1% of the total measured cross section because of our centrality cut. The representativity of the observed scaling behavior is far from certain in this case, as it is well known that data selected by cuts in distribution tails are prone to serious autocorrelation effects owing to conservation laws [15,68]. We therefore have to study the dependence of our findings on the strictness of our centrality cuts. In Fig. 15 the data for the same Xe + Sn collisions as in Fig. 9(b) have been analyzed with a slightly relaxed centrality cut, $b < 0.2b_{\max}$. The effect on the apparent value of Δ can be seen from the cumulant moments plot [Fig. 15(a)]. Relaxing the centrality condition gives an apparent scaling law with a smaller value of Δ , which is here $\Delta \approx 0.85$ instead of $\Delta = 0.89$ (see Table I). A similar dependence on the estimated centrality of collisions was observed in [44] and was interpreted in terms of a smaller excitation energy of fragmenting systems in less central collisions. However, as Fig. 15(b) shows, the Δ scaling actually begins to break down for these less central

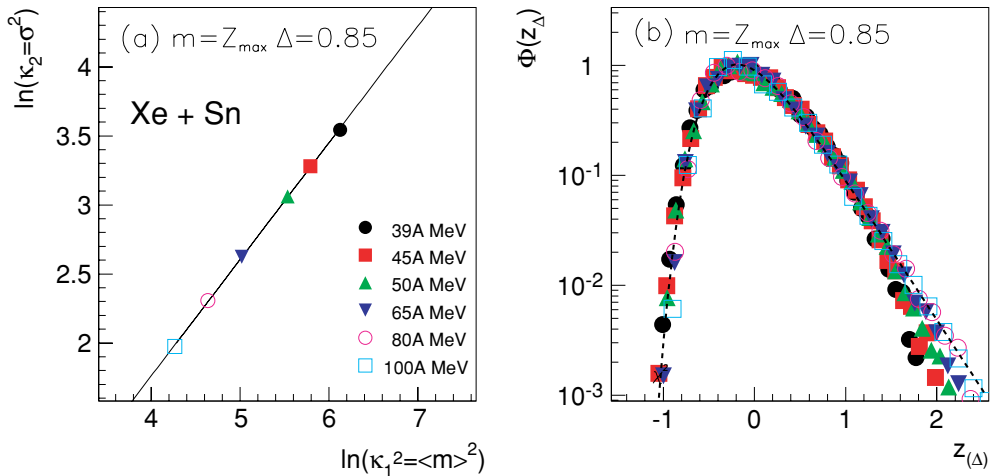


FIG. 15. (Color online) Same as Fig. 8 but for collisions with an estimated centrality of $b < 0.2b_{\max}$.

data, as can be seen in the high- $z_{(\Delta)}$ tail of the “scaling” function.

If the centrality condition is relaxed even further, $b < 0.4b_{\max}$ (Fig. 16), we first observe that now apparently all of the data for Xe + Sn are compatible with an approximate second-scaling law ($\Delta = 0.58$), without any change of scaling regime between 25A and 100A MeV. However we cannot assign the data to a single “ordered” regime because in fact this is not true Δ scaling: The different distributions no longer collapse to a universal curve [Fig. 16(b)].

Therefore we observe universal fluctuations and behavior of the Z_{\max} observable compatible with it being an order parameter for nuclear multifragmentation only for very central collisions of symmetric systems for which one may suppose a near-to-total overlap of the projectile and target in the entrance channel. We have not, up to now, observed an equivalent scaling for quasi-projectile residues in midperipheral to peripheral collisions. This may be because in such reactions the fragment production is far more sensitive to entrance channel

effects, which vary greatly as a function of the colliding nuclei and their energies. If so, a meaningful comparison between different systems is harder to achieve, at least with our rather “global” approach. In head-on collisions, in contrast, the fragmentation of the projectile and target may be virtually a statistical (although not necessarily thermal) process, far less sensitive to the details of the reaction, and therefore more amenable to reveal features that are independent of the system under study.

V. SUMMARY

We have studied nuclear multifragmentation data obtained with the INDRA 4π array for collisions of symmetric systems of total mass $A_{\text{tot}} \sim 75\text{--}400$ at bombarding energies from 25A to 100A MeV. Using the total transverse energy of light charged particles, E_{t12} , as a measure of collision violence, we deduced the evolution of these reactions with

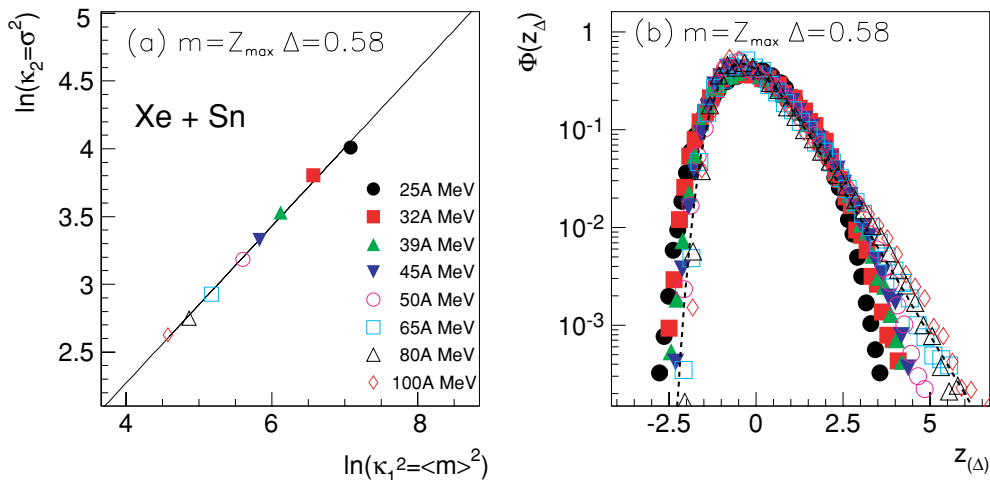


FIG. 16. (Color online) Same as Fig. 15 but for collisions with an estimated centrality of $b < 0.4b_{\max}$.

beam energy, impact parameter, and system size from the experimentally measured correlations between the charge of the largest fragment detected in each event, Z_{\max} , and E_{f12} . For all data presented in this work these correlations are dominated by reactions leading to a projectile-like fragment whose size decreases with increasing collision violence. In the case of the heaviest projectiles (Xe, Au) fission of the moderately excited quasi-projectile modify this picture. For higher excitation energies the opening of the quasi-projectile multifragmentation channel may exhibit a bimodal behavior, which has been evidenced [69] in selecting complete detection events. However, in central collisions for a few percent of the measured cross section, “heavy” residues are produced in the systems Ar + KCl, Ni + Ni and Xe + Sn, suggesting incomplete fusion of projectile and target, for beam energies that are not too high ($\leq 52A$ MeV for Ar + KCl, $\leq 40A$ MeV for Ni + Ni, and $\leq 32A$ MeV for Xe + Sn).

Using a model-independent analysis based on the theory of universal fluctuations of the order parameter for finite systems, we tested the most violent collisions for signals that the fragment production may be related to a phase transition. Following the results of [44] we first confirmed that, of the two possible order parameters for a critical fragmentation process, it is the charge (size) of the largest fragment, Z_{\max} , and not the total or IMF multiplicities M_{tot} or $M_{Z \geq 3}$, that has a behavior of the scaling properties of its fluctuations compatible with its being an order parameter for a critical fragmentation process. Indeed, we have shown that the event-by-event distribution of Z_{\max} allows us to sort data into two fluctuation-scaling regimes defined by the value of the scaling exponent Δ , which is approximately equal to 1/2 at low energies and tends toward the asymptotic value 1 at high energies with increasing total system size. These regimes are equally well characterized by a distinctive form of the scaling function $\Phi(z_{(\Delta)})$. At low energies this function, although more symmetric than that seen at higher energy, is significantly different from the Gaussian form. The deviation is quantitatively the same for the three different-sized systems (Ar + KCl, Ni + Ni, and Xe + Sn) for which we observed this low-energy regime. In the high-energy regime the scaling function is more asymmetric and tends toward the asymptotic form of the Gumbel distribution, with increasing system mass. This evolution concerns mainly the large- Z_{\max} tail of the distribution, which falls off more slowly for heavier systems, becoming exponential. For the Au + Au system $\Phi(z_{(\Delta)})$ is an almost perfect Gumbel distribution.

The bombarding energy at which the passage from one regime to the other is situated decreases as the total system mass (and charge) increases. This is contrary to the expected behavior if this transition were related to the critical temperature of the systems under study, which would increase with mass, but is nonetheless consistent with the observation of decreasing limiting temperatures for finite nuclei [64] owing to the increase in Coulomb energy for heavy nuclei. However, we can only speculate whether this is the reason for our observation, as our analysis does not depend on any model of fragment production such as supposing it to be equilibrated or thermally driven, and therefore it does not give any information on whether these conditions are met or not. Nevertheless, the data strongly suggest that the dependence on entrance channel mass and bombarding energy of the two regimes is closely linked to the disappearance of heavy residues in central collisions.

Although this analysis allows us to establish the existence of two distinct regimes in multifragmentation reactions based on the scaling properties of the fluctuations of the largest fragment, it has not given any information on the passage from one regime to the other. In the data studied so far we observe only order parameter distributions that are compatible with weakly correlated systems (i.e., far from the critical point). It may be that the general survey of a wide range of data presented here is not sufficiently detailed to reveal such features, or that data taken in small bombarding energy steps around the “transition energy” is necessary to track the evolution of the order parameter distribution. Such additional data for the Xe + Sn system have been measured recently and are currently under analysis. It is our feeling that the present work constitutes a solid basis for further study of the question of criticality in nuclear multifragmentation data.

ACKNOWLEDGMENTS

We would like to thank M. Płoszajczak for fruitful discussions and the support and interest he has shown in our work. We thank also the staff of the GANIL and GSI accelerator facilities for their support during the experiments. This work was supported by the European Community under Contract No. ERBFMGECT950083 and by the Commissariat à l’Energie Atomique, the Centre National de la Recherche Scientifique, the Ministère de l’Education Nationale, the Conseil Régional de Basse Normandie, and the Association Française des Femmes Diplômées des Universités.

-
- [1] R. T. de Souza *et al.*, Phys. Lett. **B268**, 6 (1991).
 [2] D. R. Bowman *et al.*, Phys. Rev. Lett. **67**, 1527 (1991).
 [3] C. Ogilvie *et al.*, Phys. Rev. Lett. **67**, 1214 (1991).
 [4] M. B. Tsang *et al.*, Phys. Rev. Lett. **71**, 1502 (1993).
 [5] G. F. Peaslee *et al.*, Phys. Rev. C **49**, 2271(R) (1994).
 [6] G. Bertsch and P. J. Siemens, Phys. Lett. **B126**, 9 (1983).
 [7] G. Fai, L. P. Csernai, J. Randrup, and H. Stocker, Phys. Lett. **B164**, 265 (1985).
 [8] G. Peilert *et al.*, Phys. Rev. C **39**, 1402 (1989).

- [9] J. E. Finn *et al.*, Phys. Rev. Lett. **49**, 1321 (1982).
 [10] R. W. Minich, Phys. Lett. **B118**, 458 (1982).
 [11] M. E. Fisher, Physics **3**, 255 (1967).
 [12] W. Friedman and W. G. Lynch, Phys. Rev. C **28**, 16 (1983).
 [13] R. J. Charity *et al.*, Nucl. Phys. **A483**, 371 (1988).
 [14] D. Durand *et al.*, Nucl. Phys. **A541**, 266 (1992).
 [15] W. J. Llope *et al.*, Phys. Rev. C **51**, 1325 (1995).
 [16] W. Friedman, Phys. Rev. C **42**, 667 (1990).
 [17] D. H. E. Gross, Rep. Prog. Phys. **53**, 605 (1990).

- [18] J. P. Bondorf, A. S. Botvina, A. S. Iljinov, I. N. Mishustin, and K. Sneppen, *Phys. Rep.* **257**, 133 (1995).
- [19] X. Campi, *Phys. Lett.* **B208**, 351 (1988).
- [20] A. Mekjian *et al.*, *Phys. Rev. C* **58**, 3627 (1998).
- [21] J. Richert and P. Wagner, *Phys. Rep.* **350**, 1 (2001).
- [22] L. G. Moretto and G. J. Wozniak, *Annu. Rev. Nucl. Part. Sci.* **43**, 379 (1993).
- [23] B. Lott *et al.*, *Phys. Rev. Lett.* **68**, 3141 (1992).
- [24] J. Toke *et al.*, *Phys. Rev. Lett.* **75**, 2920 (1995).
- [25] J. F. Dempsey *et al.*, *Phys. Rev. C* **54**, 1710 (1996).
- [26] G. J. Kunde *et al.*, *Phys. Rev. Lett.* **77**, 2897 (1996).
- [27] Y. Larochele *et al.*, *Phys. Rev. C* **53**, 823 (1996).
- [28] N. Marie *et al.* (INDRA Collaboration), *Phys. Lett.* **B391**, 15 (1997).
- [29] J. Łukasik *et al.* (INDRA Collaboration), *Phys. Rev. C* **55**, 1906 (1997).
- [30] R. Nebauer *et al.* (INDRA Collaboration), *Nucl. Phys.* **A658**, 67 (1999).
- [31] E. Plagnol *et al.* (INDRA Collaboration), *Phys. Rev. C* **61**, 014606 (1999).
- [32] T. Lefort *et al.* (INDRA Collaboration), *Nucl. Phys.* **A662**, 397 (2000).
- [33] B. Djerroud *et al.*, *Phys. Rev. C* **64**, 034603 (2001).
- [34] J. D. Frankland *et al.* (INDRA Collaboration), *Nucl. Phys.* **A689**, 905 (2001).
- [35] J. D. Frankland *et al.* (INDRA Collaboration), *Nucl. Phys.* **A689**, 940 (2001).
- [36] B. Borderie *et al.* (INDRA Collaboration), *Phys. Rev. Lett.* **86**, 3252 (2001).
- [37] N. Bellaize *et al.* (INDRA Collaboration), *Nucl. Phys.* **A709**, 367 (2002).
- [38] J. Colin *et al.* (INDRA Collaboration), *Phys. Rev. C* **67**, 064603 (2003).
- [39] J. L. Charvet, R. Dayras, D. Durand, O. Lopez, D. Cussol, D. Doré, L. Nalpas, A. van Lauwe, and C. Volant, *Nucl. Phys.* **A730**, 431 (2004).
- [40] R. Botet, M. Płoszajczak, and V. Latora, *Phys. Rev. Lett.* **78**, 4593 (1997).
- [41] R. Botet and M. Płoszajczak, *J. Sol-Gel Sci. Technol.* **15**, 167 (1999).
- [42] R. Botet and M. Płoszajczak, *Phys. Rev. E* **62**, 1825 (2000).
- [43] R. Botet and M. Płoszajczak, *Nucl. Phys. Proc. (Suppl.)* **92**, 101 (2001), hep-ph/0009233.
- [44] R. Botet *et al.*, *Phys. Rev. Lett.* **86**, 3514 (2001).
- [45] E. Gumbel, *Statistics of Extremes* (Columbia University Press, New York, 1958).
- [46] R. Botet and M. Płoszajczak, *Phys. Rev. Lett.* **69**, 3696 (1992).
- [47] J. Pouthas *et al.*, *Nucl. Instrum. Methods A* **357**, 418 (1995).
- [48] J. C. Steckmeyer *et al.*, *Nucl. Instrum. Methods A* **361**, 472 (1995).
- [49] J. Pouthas *et al.*, *Nucl. Instrum. Methods A* **369**, 222 (1996).
- [50] G. Tăbăcaru *et al.* (INDRA Collaboration), *Nucl. Instrum. Methods A* **428**, 379 (1999).
- [51] M. Pârlog *et al.* (INDRA Collaboration), *Nucl. Instrum. Methods A* **482**, 674 (2002).
- [52] M. Pârlog *et al.* (INDRA Collaboration), *Nucl. Instrum. Methods A* **482**, 693 (2002).
- [53] A. Trzciski *et al.* (INDRA and ALADIN Collaborations), *Nucl. Instrum. Methods A* **501**, 367 (2003).
- [54] V. Métivier *et al.* (INDRA Collaboration), *Nucl. Phys.* **A672**, 357 (2000).
- [55] F. Bocage *et al.* (INDRA Collaboration), *Nucl. Phys.* **A676**, 391 (2000).
- [56] A. Ono, S. Hudan, A. Chbihi, and J. D. Frankland, *Phys. Rev. C* **66**, 014603 (2002).
- [57] A. Le Fèvre *et al.* (INDRA and ALADIN Collaborations), *Nucl. Phys.* **A735**, 219 (2004).
- [58] J. D. Frankland *et al.* (INDRA Collaboration), in *Proceedings of the XL International Winter Meeting on Nuclear Physics*, edited by I. Iori (Ricerca Scientifica ed Educazione Permanente, Milan, 2002), nucl-ex/0202026.
- [59] C. Cavata *et al.*, *Phys. Rev. C* **42**, 1760 (1990).
- [60] D. Sisan *et al.*, *Phys. Rev. C* **63**, 027602 (2001).
- [61] J. Lecolley *et al.*, *Phys. Lett.* **B391**, 317 (1994).
- [62] H. Jaqaman, A. Mekjian, and L. Zamick, *Phys. Rev. C* **29**, 2067 (1984).
- [63] S. Levit and P. Bonche, *Nucl. Phys.* **A437**, 426 (1985).
- [64] J. B. Natowitz *et al.*, *Phys. Rev. C* **65**, 034618 (2002), nucl-ex/0106016.
- [65] B. Roe, *Probability and Statistics in Experimental Physics* (Springer-Verlag, New York, 1992).
- [66] R. Botet and M. Płoszajczak (in preparation).
- [67] J. M. Carmona, J. Richert, and P. Wagner, *Phys. Lett.* **B531**, 71 (2002).
- [68] L. Phair *et al.*, *Nucl. Phys.* **A548**, 489 (1992).
- [69] B. Tamain *et al.* (INDRA Collaboration), in *Proceedings of the IWM2003 (International Workshop on Multifragmentation and Related Topics)* (GANIL and INFN, Caen, 2003).